Supplemental

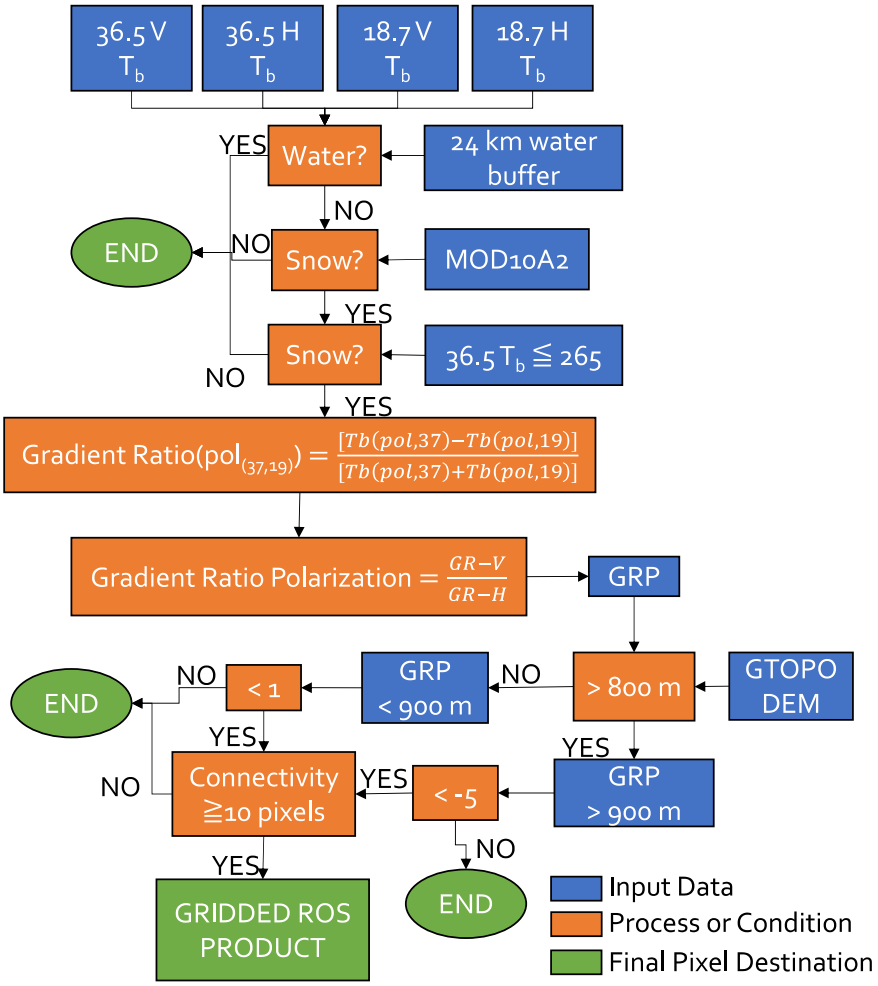

Figure S1. Schematic of workflow used to derive gridded daily PM ROS product.

Supplemental 1. GRP Threshold Selection

Algorithm outputs with a GRP threshold of 1, used to classify ROS events, were found to detect an anomalously high number of ROS events per year (i.e. >120 days) at higher elevations above 900 m (figure S2). This apparent ROS overestimation at higher elevations was attributed to the strong GRP sensitivity to variations in snow density (Alford, 1967; Pistocchi, 2016), where the GRP threshold increases with decreasing snow density (Langlois et al., 2017). A discrete increase in apparent GRP overestimated ROS pixels at elevations between 900 - 2700 m is illustrated in figure S2. To address potential ROS classification errors we applied two different GRP thresholds for varying snow conditions at lower and higher elevations. We applied a GRP

threshold of 1 (Dolant et al., 2016) for elevations below 900 m and an alternate GRP threshold of -5 (Langlois et al., 2017) for elevations above 900 m. Figure S2 also portrays the apparent ROS overestimation at elevations between 0 and 200 m, addressed in section 4.2. Finally, ROS affected pixels below a minimum spatial connectivity threshold of 10 pixels at each daily time step were screened from the data record to spatially distinguish more extensive ROS occurrences from smaller isolated events. The resulting elevation threshold reduced anomalous ROS pixels above 900 m elevation by 100 %, while the spatial connectivity filter reduced the number of isolated locations with ROS below 900 m by 63 % (figure S2).

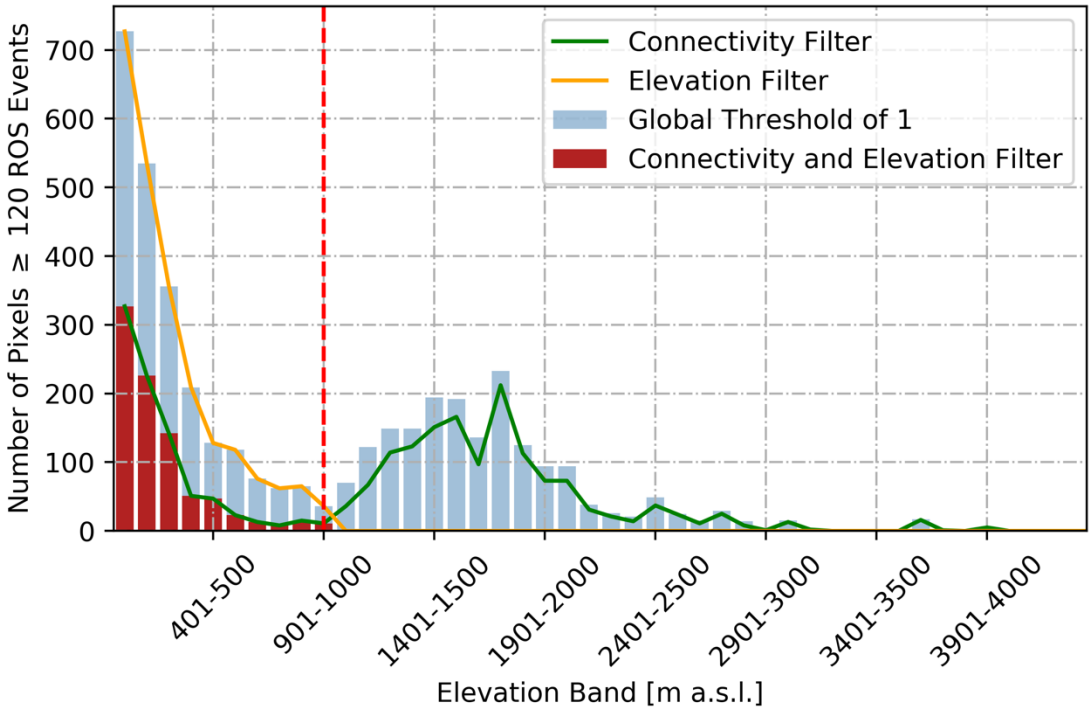

Figure S2. Distribution of ROS days per year by mean elevation band, vertical red line (900 m) denotes the minimum elevation where the GRP threshold of -5 was used.

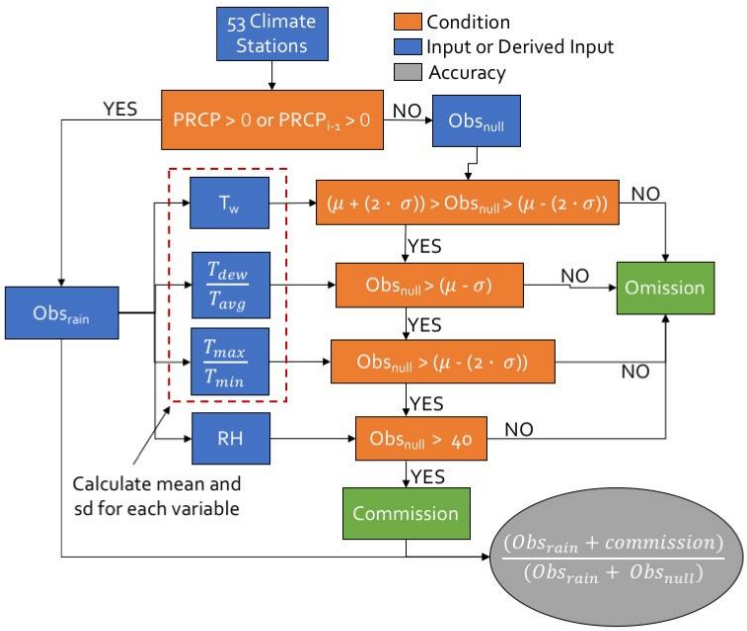

Figure S3. Workflow schematic for Tier 2 validation.

Supplemental 2. Description of Tier-2 temperature metrics

We created three temperature driven variables to be used as a proxy for rainfall conditions. These metrics included wet bulb temperature (T_w), the ratio between daily dew point temperature (T_{dew}) and average temperature (T_{dew}/T_{avg}) and the ratio between maximum temperature (T_{max}) and minimum temperature (T_{min}) (T_{max}/T_{min}). The precipitation proxies are used as indicators for atmospheric moisture and energy.

Because air temperature can be highly variable during ROS events (Dolant et al., 2017), we chose a more stable approach of T_w, where T_w is a proxy for precipitation and ROS occurrence. This served two purposes: 1) T_w constrained the feasibility that precipitation would fall as liquid and 2) T_w provided a better indicator of precipitation phase (Sims and Liu, 2015). The derivation of T_w can be found in supplemental 3. The T_{dew}/T_{avg} metric was used to represent the dew point depression and the amount of moisture in the atmosphere (Feld et al., 2013), providing a normalized value for the 'degree of saturation' in the atmosphere. The T_{max}/T_{min} metric was used as a proxy for cloudiness based on the assuming cloudier conditions decreased radiative heating and cooling of the land surface and the associated daily temperature amplitude (Tomsett and

Toumi, 2000). Cloudiness was defined as a relative percentage from 0-100% ranging between clear sky conditions and complete cloud cover.

Using Obs_{rain}, the mean (μ) and standard deviation (σ) were created for each precipitation proxy to constrain Obs_{null}. If Obs_{null} met all of the requirements set by the precipitation proxies, the conditions were identified as feasible for precipitation. ROS days which met all of the constraining conditions set by Obs_{rain} were classified as commission whereas all Obs_{null} observations that did not meet the defined conditions were classified as omission. The final ROS accuracy was calculated as a percentage of the sum of Obs_{rain} and commission days divided by the total number of classified ROS days.

Supplemental 3. Derivation of wet bulb

To derive T_w, we first calculated vapor pressure [E] from T_{dew}:

$$E = 6.11 \cdot 10^{\frac{7.5 \cdot T_{dew}}{237.7 + T_{dew}}} \qquad \text{Eq. 1}$$

Using E, T_{dew}, T_{avg}, and station pressure [mb] (STP), Tw can then be derived by the following (Sullivan and Sanders 1977):

$$T_w = \left(0.00066 \cdot STP + T_{avg}\right) + \frac{\left[\frac{4098 \cdot E}{(T_{dew}+237.7)^2 \cdot T_{dew}}\right]}{\left[\frac{(0.00066 \cdot STP)+(4098 \cdot E)}{(T_{dew}+237.7)^2}\right]} \qquad \text{Eq. 2}$$

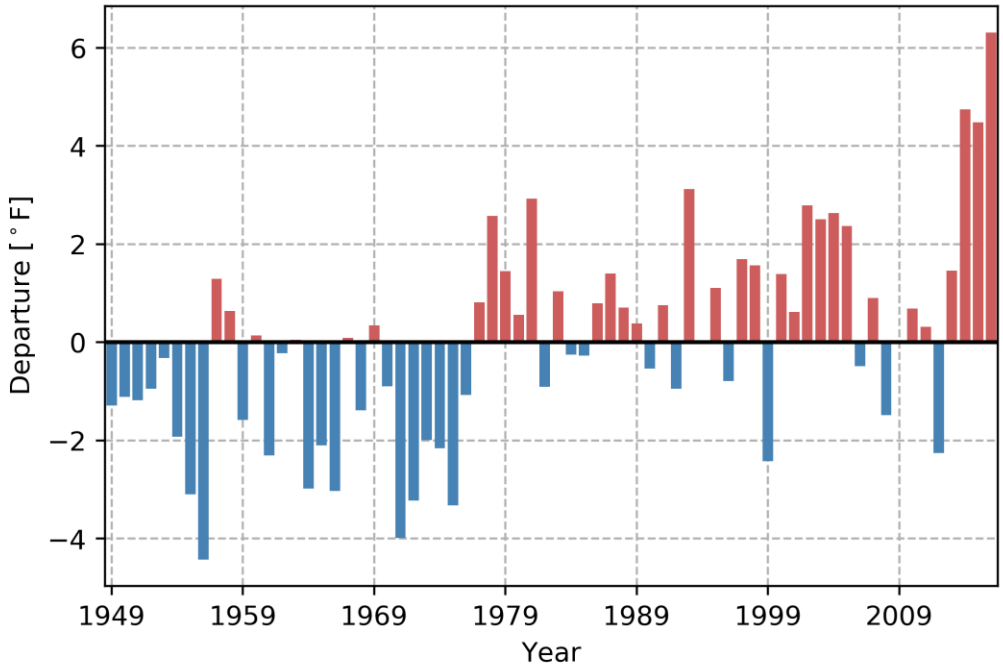

Figure S4. Time-series of mean annual temperature departures across the state of Alaska from 1949-2016; data are provided by the Alaska Climate Data Research Center.

Supplemental 4. Limitations in validating PM derived ROS

Validating satellite derived ROS is limited by the number and quality of in situ meteorological observations in boreal and arctic regions; a region with limited access, severe climate conditions and sparse weather station networks. The Tier-1 assessment included multiple precipitation observations and was the most inclusive and reliable form of validation used in this study, despite being limited to a single set of ground observations for a single location in central Alaska. The Tier-1 results also showed the limitation of in situ precipitation observations to exclusively validate ROS; this reflects uncertainty in precipitation measurements and reporting due to sensor limitations, wind redistribution effects, blockage of gauges/sensors, biases introduced during post-thaw events, and human error (Merenti-Valimaki 2001, Martinaitis *et al* 2015, Grossi *et al* 2017). Discrepancies between the satellite retrievals and in situ precipitation measurements may also reflect differences in both the spatial footprint of observations and the physical phenomena being measured. For example, the PM derived ROS signal reflects changes in surface wetness that may be caused by either direct rainfall inputs or surface snowmelt driven by sensible, turbulent and or latent heat fluxes (Marks *et al.* 1998). The Tier-1 validation results

indicated that the majority of ROS events occur in early November at the Fairbanks station location. This early occurrence and the large number of reported observations of fog suggests that latent and turbulent heat flux contribute to the ROS observations during periods with no measurable precipitation; these results also suggest that fog followed by wind may be a valid proxy for ROS occurrence. However, no attempt was made to differentiate between fog and freezing fog, as freezing fog would not contribute to wet snow conditions. Measured precipitation provided the highest omission error during each year of record, except for WY 2014, suggesting that a number of ROS events possessed only trace amounts of precipitation that were below the detection level of the PAFA station. Unfortunately, the Tier-1 validation was restricted to the PAFA station since it was the only record documented as a high-quality data set by human observers.

Tier-2 validation was applied across the Alaska domain, with only 19 % of the PM derived ROS days showing measured precipitation (Obs_{rain}). Two factors contribute to this lack of coincident observations. First, rain is not the singular factor determining wet snow surface conditions, which are frequently due to energy exchange processes that can occur before, during and after, and sometimes independently, of rain events. These processes include turbulent exchange and sensible and latent heat fluxes, which are the primary source of snowpack melt energy flux during the winter accumulation phase of high latitude snowpacks. The period for ROS detection in this study was constrained between Nov-Mar when solar insolation is relatively low, so that solar radiation is not the primary source of snowmelt energy. Second, measurement technologies and the arduous quality checking (QA and QC) process required to effectively discriminate between rain, snow and mixed precipitation data are nearly nonexistent for Alaska climate records; the first observer data for the Fairbanks site used in the Tier-1 validation was the only record of this type we could find (Grossi et al., 2017; Martinaitis et al., 2015).

References

Alford, D., 1967. Density variations in alpine snow. J. Glaciol. 6.

Dolant, C., Langlois, A., Brucker, L., Royer, A., Roy, A., Montpetit, B., 2017. Meteorological inventory of rain-on-snow events in the Canadian Arctic Archipelago and satellite detection assessment using passive microwave data. Phys. Geogr. 3646, 1–17. doi:10.1080/02723646.2017.1400339

Dolant, C., Langlois, A., Montpetit, B., Brucker, L., Roy, A., Royer, A., 2016. Development of a

rain-on-snow detection algorithm using passive microwave radiometry. Hydrol. Process. 30, 3184–3196. doi:10.1002/hyp.10828
Feld, S.I., Cristea, N.C., Lundquist, J.D., 2013. Representing atmospheric moisture content along mountain slopes: Examination using distributed sensors in the Sierra Nevada, California. Water Resour. Res. 49, 4424–4441. doi:10.1002/wrcr.20318
Grossi, G., Lendvai, A., Peretti, G., Ranzi, R., 2017. Snow precipitation measured by gauges: Systematic error estimation and data series correction in the central Italian Alps. Water (Switzerland) 9, 1–14. doi:10.3390/w9070461
Langlois, A., Johnson, C.A., Montpetit, B., Royer, A., Blukacz-Richards, E.A., Neave, E., Dolant, C., Roy, A., Arhonditsis, G., Kim, D.K., Kaluskar, S., Brucker, L., 2017. Detection of rain-on-snow (ROS) events and ice layer formation using passive microwave radiometry: A context for Peary caribou habitat in the Canadian Arctic. Remote Sens. Environ. 189, 84–95. doi:10.1016/j.rse.2016.11.006
Martinaitis, S.M., Cocks, S.B., Qi, Y., Kaney, B.T., Zhang, J., Howard, K., 2015. Understanding Winter Precipitation Impacts on Automated Gauge Observations within a Real-Time System. J. Hydrometeorol. 16, 2345–2363. doi:10.1175/JHM-D-15-0020.1
Merenti-Valimaki, H.-L., 2001. Present weather: comparing human observations and one type of automated sensor. Meteorol. Appl. 8, 491–496.
Pistocchi, A., 2016. Simple estimation of snow density in an Alpine region. J. Hydrol. Reg. Stud. 6, 82–89. doi:10.1016/j.ejrh.2016.03.004
Sims, H.E., Liu, G., 2015. A Parameterization of the Probability of Snow – Rain Transition. J. Hydrometeorol. 16, 1466–1477. doi:10.1175/JHM-D-14-0211.1
Sullivan J, and Sanders L D 1977 Method for obtaining wet-bulb temperature by modifying the psychometric formula, *NOAA Technical Memorandum* **EDS BOMAP-11**
Tomsett, A.C., Toumi, R., 2000. Diurnal temperature range and rainfall probability over the United Kingdom. Geophys. Res. Lett. 27, 1279–1282. doi:10.1029/1999GL011335